IEEE Access
Multidisciplinary | Rapid Review | Open Access Journal

Received October 22, 2018, accepted November 15, 2018, date of publication November 21, 2018,
date of current version December 31, 2018.

Digital Object Identifier 10.1109/ACCESS.2018.2882678

Distributed Hierarchical Control of AC Microgrid Operating in Grid-Connected, Islanded and Their Transition Modes

XIAOCHAO HOU[1,2], YAO SUN[1,2], (Member, IEEE), JINGHANG LU[3], (Member, IEEE), XIN ZHANG[3], (Member, IEEE), LEONG HAI KOH[4], MEI SU[1,2], AND JOSEP M. GUERRERO[5], (Fellow, IEEE)

[1]School of Information Science and Engineering, Central South University, Changsha 410083, China
[2]Hunan Provincial Key Laboratory of Power Electronics Equipment and Grid, Changsha 410083, China
[3]School of Electrical and Electronic Engineering, Nanyang Technological University, Singapore 639798
[4]Energy Research Institute, Nanyang Technological University, Singapore 639798
[5]Department of Energy Technology, Aalborg University, 9220 Aalborg, Denmark

Corresponding author: Jinghang Lu (lujh@ntu.edu.sg)

This work was supported in part by the National Natural Science Foundation of China under Grant 61622311, in part by the Joint Research Fund of Chinese Ministry of Education under Grant 6141A02033514, in part by the Natural Science Foundation of Hunan Province of China under Grant 2016JJ1019, in part by the Project of Innovation-driven Plan in Central South University under Grant 2019CX003, and in part by the Hunan Provincial Innovation Foundation for Postgraduate.

ABSTRACT In this paper, a distributed hierarchical control is proposed for ac microgrid, which could apply to both grid-connected (GC) mode and islanded (IS) mode as well as mode transitions. The control includes three control levels: 1) the basic droop control is adopted as the primary control; 2) the secondary control is based on the distributed control with a leaderâĂ"follower consensus protocol; and 3) the tertiary level is a mode-supervisory control, which manages the different control targets of four operation modes. Under the proposed control framework, the following targets are achieved: 1) the frequency/voltage recovery and accurate power sharing in IS mode; 2) flexible power flow regulation between utility-grid and microgrid in GC mode; 3) universal control strategy from GC to IS modes without control switching; and 4) smooth active-synchronization from IS mode to GC mode. In this sense, the proposed method can adapt to all four operation modes of microgrid. Compared with central-standard hierarchical control, the proposed method only requires local neighbor-to-neighbor interaction with a sparse distributed communication network. Thus, the scalability, flexibility, reliability, and robustness are greatly improved in practical application. In addition, stability analysis is added to facilitate the control parameter designs, and substantial simulation cases are provided to validate the control feasibility, link-failure-resiliency, and plug-and-play capability.

INDEX TERMS Distributed coordination, hierarchical control, microgrid, seamless transition.

I. INTRODUCTION

The concept of microgrid has been early defined to cope with the high penetration of various distributed generations (DGs) [1]. Then, this promising solution of microgrid is gradually an effective support for main utility-grid [2], [3]. As a distributed power network, microgrid is capable of operating in grid-connected mode (GC) and islanded mode (IS) to realize grid-support, islanded power supplies and ancillary services [4], [5].

In microgrid, distributed generations (DGs) are always connected to power network via power inverter interfaces. The inverter-interfaced DGs are mainly controlled as current controlled sources or voltage controlled sources [6], [7]. In the GC mode, DGs commonly act as current controlled sources to retain a high grid-current quality and a fast dynamic response in the photovoltaic [8] and wind [9] generation systems. However, this current controlled DGs cannot work alone without the voltage/frequency support from utility-grid. To enhance the dynamic and stability performances, various variants of grid-feeding DGs are elaborated in [10], [11].

In IS mode, the inverter-interfaced DGs often work as voltage-controlled sources [6], [7]. As system voltage and frequency are not determined by utility-grid, DGs should take charge of the voltage/frequency stability. Moreover, the power sharing should be guaranteed according to

their individual ratings to avoid circulating currents among DGs [12], [13].

To ensure the power sharing and voltage/frequency stability, the droop control method is mostly applied by mimicking the behavior of synchronous generator [14], [15]. Under the droop control frame, the frequency and voltage-amplitude references of each DG are established according to its output active and reactive power, respectively. Since communications are not necessary for synchronizing DGs, the droop-based has advantages in reliability and flexibility. In addition, the droop-controlled microgrid [14]–[17] can operate in both GC mode and IS mode, but it cannot realize a seamless mode-transition from IS mode to GC mode, and there are some potential weaknesses in its practical applications:

- *Inaccurate power sharing*: In IS mode, accurate reactive power sharing cannot be achieved because of the unbalanced feeder impedances [16];
- *Frequency and voltage deviations*: In IS mode, the voltage/frequency deviation from nominal values is an unavoidable drawback of droop control [17];
- *Uncontrolled grid-injected power flow*: In GC mode, the active and reactive power flow between microgrid and utility-grid is sensitive to grid operation conditions [18], such as, grid voltage and frequency variations;
- *Difficult to realize mode-transition from IS to GC mode*: In seamless mode-transition from IS mode to GC mode, a central synchronization controller is required to reconnect a whole networked microgrid to utility-grid by a real-time high-bandwidth communication network, which is not cost-effective in practice [19].

Recently, some measures have been taken to overcome the above drawbacks of droop control. For the first issue, to ameliorate reactive power sharing precision, virtual impedance is a promising method [16], [17], but accurate power sharing cannot be exactly attained. For the second issue of frequency/voltage deviations, distributed control frames [20], [22] are often utilized for voltage and frequency recovery in IS mode. But little literature analyzes the application of distributed control in GC mode. For the third issue, to fix the power flow between microgrid and utility-grid in GC mode, [18] presents a feed-forward-based control of grid real-time frequency/voltage amplitudes. Although power flow control is ensured for droop-controlled DGs with improved stability, these feed-forward terms would cause an adverse influence in IS mode. Lastly, to maintain a smooth mode-synchronization from IS to GC mode, the point of grid-connection (PCC) must be synchronized with utility-grid. Especially for a meshed microgrid with multiple DGs, the synchronization compensation signals are transmitted from a central controller to all DGs by a communication network [23]–[25]. It would result in high communication costs, and this star communication architecture is vulnerable to single point failure. Thus, central control is impractical for complex microgrid network consisted by a number of DGs. Generally, in [15]–[25], each of them only deals with a single research point and compensates one limitation of the droop mechanism. They lack a systematic perspective to consider all required performances for overall operation modes. Therefore, they are limited in practical applications.

Nowadays, the hierarchical control frame [26], [27] is referred to a general standardization of microgrid control [28]. All operation targets are assigned to multiple separated control levels with different time scales [33]. In [26], [27], this typical hierarchical structure consists of primary, secondary and tertiary control. The primary control is responsible for the local voltage and frequency supports and offers power-sharing capability. The secondary control, also as a microgrid centralized controller, restores the voltage and frequency deviations and ensures a high voltage quality. Tertiary control manages the power flowing interaction between the whole microgrid and utility-grid. Although this central-standard hierarchical control is widely applied in DC Microgrid [29], Hybrid AC/DC Microgrid [30], and community microgrid [31], [32], the previous research merely considered all four operation modes.

In this study, a distributed hierarchical control is introduced, which guarantees a complete operation in four modes with a seamless mode-transition capability [34]. All control targets are involved in three control levels: **i**) the primary droop is utilized as a backup control, which guarantee the normal operation even in case of communication failures; **ii**) the secondary distributed control maintains the power sharing and voltage/frequency recovery; **iii**) the tertiary control prescribes the control tasks of each mode according to a mode-supervisory controller, which provides seamless transitions from one mode to the other.

The proposed distributed hierarchical control framework has many merits than other control-based framework [33]. Compared to the primary droop control [14], [15] or distributed control framework [20], [22], the proposed control framework combines the merits of the primary droop control, secondary distributed control, and tertiary mode-supervisory control. Thus, the proposed control strategies can adapt to four operation modes. Meanwhile, the favorable plug-and-play and link-failure-resiliency capability are more outstanding with the proposed control framework, which cannot be realized with master-slave control or central-control framework [28], [33]. Compared with existing standardized hierarchical methods [26], [27], the proposed method has some obvious features:

- *Suitable for all modes.* The original hierarchical control in [26] and [27] only focuses on the GC mode and IS mode. Alternatively, the proposed distributed hierarchical can be applied to all operation modes (GC mode, IS mode and mode transitions).
- *Sparse low-bandwidth communication.* In [26] and [27], the secondary control is based on a centralized controller, which is vulnerable to single point failure. Instead, this study introduces a distributed control in

the secondary control, which could tolerate some types of single point failure. Meanwhile, the communication complexity and burden are greatly reduced.

- *Better Practicability.* The high system reliability, flexibility and plug-and-play functionality are possessed for practical microgrids.

Compared to the previous conference version [34], three points are highlighted in this work. First, a universal distributed hierarchical control framework is exploited for operation in grid-connected, islanded and the transition modes between them. In the conference paper, the secondary distributed consensus algorithm was proposed. But, the three-level distributed hierarchical control strategies have not been mentioned, which are clearly presented now. In addition, the stability analysis is added to provide a guideline for parameter designs in section IV. Finally, more testing cases are added to verify the plug-and-play and the link-failure-resiliency capability in Sections V.

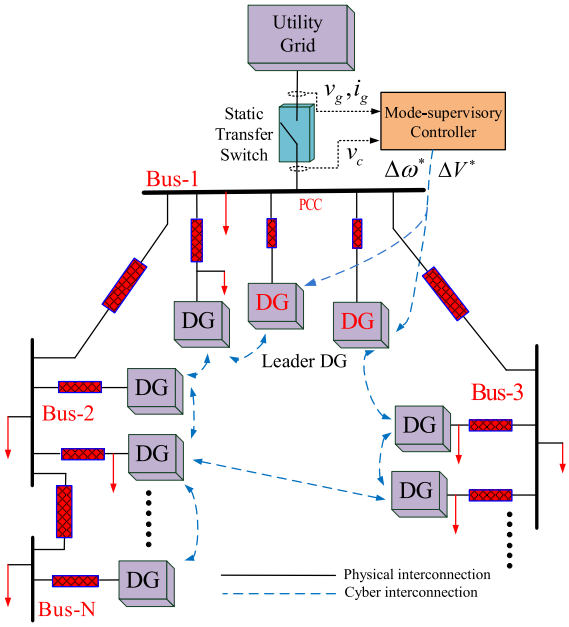

FIGURE 1. AC microgrid with a sparse distributed communication network.

II. SYSTEM CONFIGURATION OF AC MICROGRID

A. PHYSICAL AND CONTROL STRUCTURE OF AC MICROGRID

Fig. 1 presents a typical topology of an AC microgrid, in which the physical structure contains multiple DGs, buses, transmission lines and loads. The distributed communication cyber overlays the physical power network. Only local neighbor-to-neighbor communication interaction is allowed for each DG. Moreover, all DGs should be connected to this distributed communication network with at least one spanning tree. Comparing with central-based control, the distributed control scheme utilizes a sparse communication.

A static transfer switch (STS) is required to connect the PCC with utility-grid. Normally, the microgrid works in the grid-connected mode with STS $= 1$. When the power quality of utility-grid does not meet the operation criteria, the STS will switch to 0, and the islanded microgrid is formed. After the restoration of utility-grid, the active synchronization algorithm would be activated to reconnect microgrid back to utility-grid. To guarantee uninterruptible power supplies and reduce the rush currents, the seamless transition strategy between the two modes has a great significance.

In Fig.1, DGs are classified into two types: leader DGs and follower DGs. Leader DGs are chosen with a higher power-rating and installed near to PCC. Most of rest DGs work as follower DGs.

A mode-supervisory controller is installed around the STS. It just transmits the compensation signals to a few leader DGs near PCC while the remaining DGs exchanged the signals with their neighbor DGs by adopting the distributed control strategy. In this way, the communication failure at one node does not affect the normal microgrid operation, which is in contrast with the traditional centralized controller. As a result the system reliability and stability are remarkably enhanced. In addition, by using the proposed mode-supervisory controller, the communication burden of tertiary control is greatly reduced as well. Thus, the tertiary mode-supervisory control of this work is not a traditional centralized control. From the status of the STS, different compensation signals are dictated to accomplish control targets in four-modes (GC mode, IS mode, and transitions between them). Finally, all DGs work towards the common consensus objects prescribed by the mode-supervisory controller under different modes.

B. CONTROL TARGETS UNDER DIFFERENT MODES

Under different operation states of GC mode, IS mode and mode transitions, the control targets are summarized [16]–[19]:

- *Accurate load power sharing in IS mode.*

The load power demand should be properly shared among DGs according to their power capacities;

- *Excellent voltage/frequency quality in IS mode.*

The voltage/frequency deviations caused by droop control should be restored to ensure a satisfactory voltage quality;

- *Adjustable grid-injected power flow in GC mode.*

The grid-injected power should be adjusted flexibly between the microgrid and utility-grid, and the injected power should be immune to grid-voltage variations;

- *Seamless transition from GC mode to IS mode.*

Unified control strategy should be constructed to avoid the control structure reconfiguration from GC mode to IS mode;

- *Desired synchronization from IS mode to GC mode.*

A smooth transition should be enabled to provide a zero-inrush-current during the pre-synchronization.

For the four operation modes, above overall performances should be considered from a systematic view in Fig. 2.

III. PROPOSED DISTRIBUTED HIERARCHICAL CONTROL

The overall control block diagram of proposed distributed hierarchical control is shown in Fig. 3. This control scheme

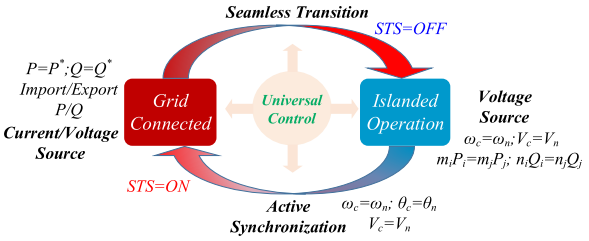

FIGURE 2. Control targets of four modes.

has three main control levels: **i**) the primary droop control; **ii**) the secondary distributed leader-follower control; **iii**) the tertiary mode-supervisory control.

A. PRIMARY DROOP CONTROL FOR INVERTER-BASED DGS

To proportionately share the load power demand and support the frequency/voltage stability, the conventional droop control is a main technique with local information feedback [14], [15].

$$\omega_i = \omega^* - m_i P_i \tag{1}$$

$$V_i = V^* - n_i Q_i \tag{2}$$

where ω_i and V_i are the angular frequency and voltage amplitude references of an inverter-based *i-th* DG, respectively. ω^* and V^* imply the values of ω and V at no load. P_i and Q_i are output active power and reactive power of *i-th* DG. m and n are droop-coefficients of P-ω and Q-V control, respectively.

Fig. 4 presents a typical control scheme of an inverter-based DG, which includes three control loops: droop-control loop, inner-voltage-loop and inner-current-loop. Furthermore, a virtual-impedance control is used to guarantee a mainly inductive output impedance [15].

B. SECONDARY DISTRIBUTED LEADER-FOLLOWER CONTROL

The distributed coordination involves two regulation parts: frequency-consensus and voltage-consensus.

For inverter-based DG-i, the frequency-active power control is designed by combining primary frequency-droop and secondary-frequency control as

$$\omega_i = \omega^* - m_i P_i + \Delta\omega_i \tag{3}$$

$$k_\omega \frac{d\Delta\omega_i}{dt} = \sum_{j\in N, j\neq i} a_{ij}(\Delta\omega_j - \Delta\omega_i) + \gamma_i(\Delta\omega^* - \Delta\omega_i) \tag{4}$$

where $\Delta\omega_i$ is an additional regulation term for the primary droop control in (3). Equation (4) is a secondary distributed frequency control. a_{ij} represents a distributed communication link. If there is an adjacency communication link from DG-j to DG-i, $a_{ij} = 1$ is set. If DG-i is chosen as a leader-DG, $\gamma_i = 1$; Otherwise, $\gamma_i = 0$. $\Delta\omega^*$ is a compensation signal from tertiary mode-supervisory control. k_ω is a positive control gain, which can adjust the response speed of the secondary frequency control.

From (4), $\Delta\omega_i = \Delta\omega_j = \Delta\omega^*$ in steady state, which implies that a uniform frequency shifting is obtained for all DGs. Fig. 5 exhibits the primary frequency droop control before and after the secondary distributed-control for two DGs. From Fig. 5, the secondary distributed control action can be regarded as a frequency recovery with a shifting of $\Delta\omega_i$.

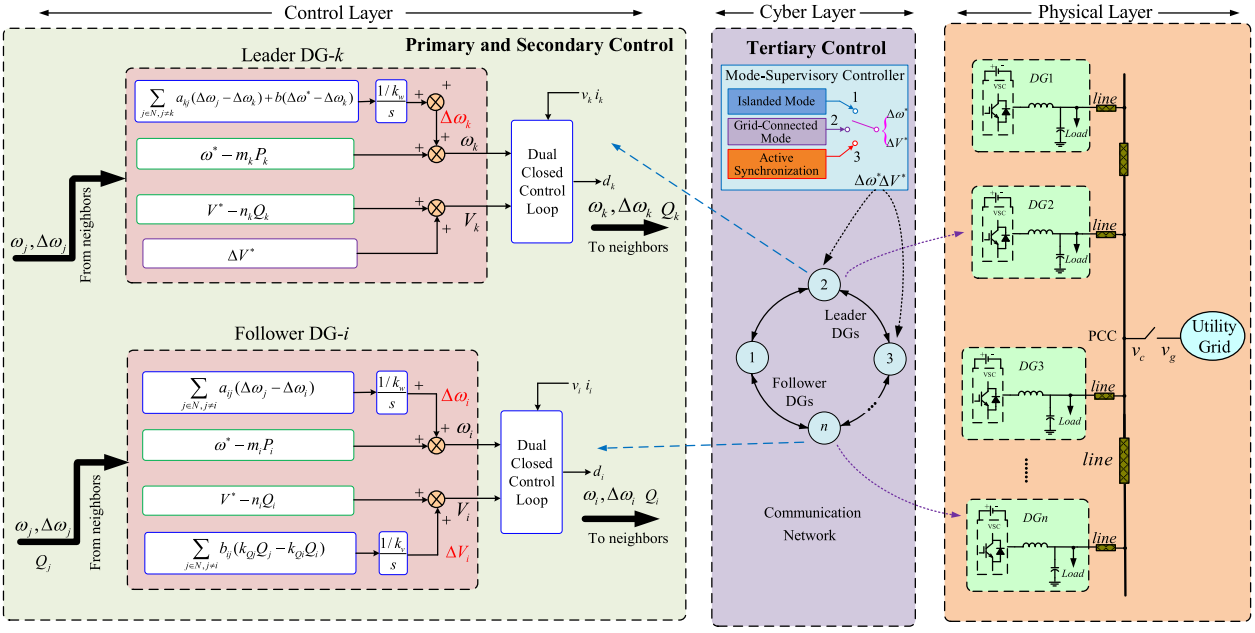

FIGURE 3. Proposed distributed hierarchical control scheme (leader DG-k; follower DG-i).

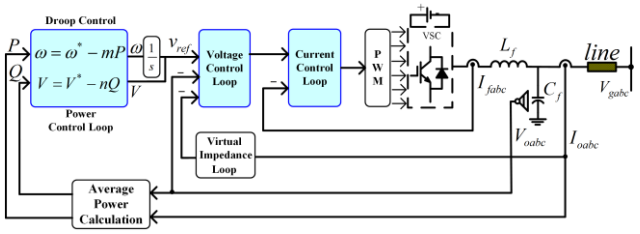

FIGURE 4. A typical control scheme of an inverter-based DG.

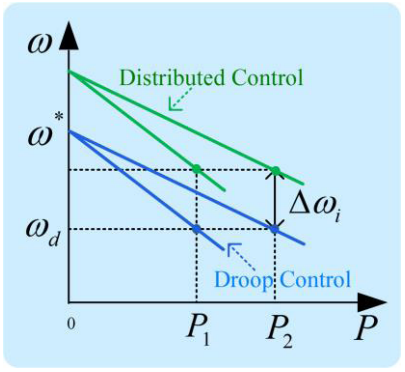

FIGURE 5. A uniform frequency shifting for primary droop control.

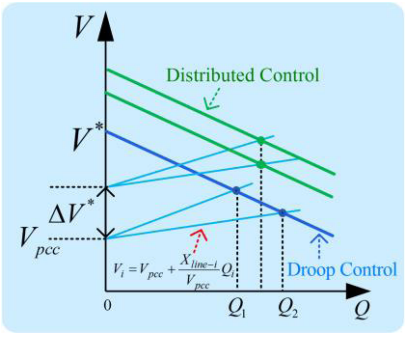

FIGURE 6. Reactive power sharing under Q-V droop control.

For inverter-based DG-i, the voltage-reactive power control is constructed by combining primary voltage-droop and secondary distributed-voltage control as

$$V_i = V^* - n_i Q_i + \Delta V_i + \beta_i \Delta V^* \tag{5}$$

$$k_v \frac{d\Delta V_i}{dt} = \sum_{j \in N, j \neq i} b_{ij}(k_{Qj} Q_j - k_{Qi} Q_i) \tag{6}$$

where (6) is a secondary distributed voltage control. b_{ij} represents a distributed communication link. k_v is a positive control gain. ΔV^* is a voltage compensation signal from tertiary mode-supervisory control. For a leader DG-k, $\beta_k = 1$ and $b_{kj} = 0$. While for rest follower-DGs, $\beta_i = 0$ and $b_{ij} = 1$. That is, only leader-DG-k is responsible for the PCC voltage, and other follower-DGs participate in reactive-power sharing.

Fig. 6 depicts the reactive-power sharing under Q-V droop control before and after combining the secondary distributed voltage control for two DGs [35]. Since the mismatch line impedances $X_{line-1} > X_{line-2}$, reactive power is not shared under the primary voltage droop control. But, with the help of the secondary distributed voltage control, $k_{Qj}Q_j = k_{Qi}Q_i$ in steady state from (6), which implies that accurate reactive power sharing is obtained among all DGs.

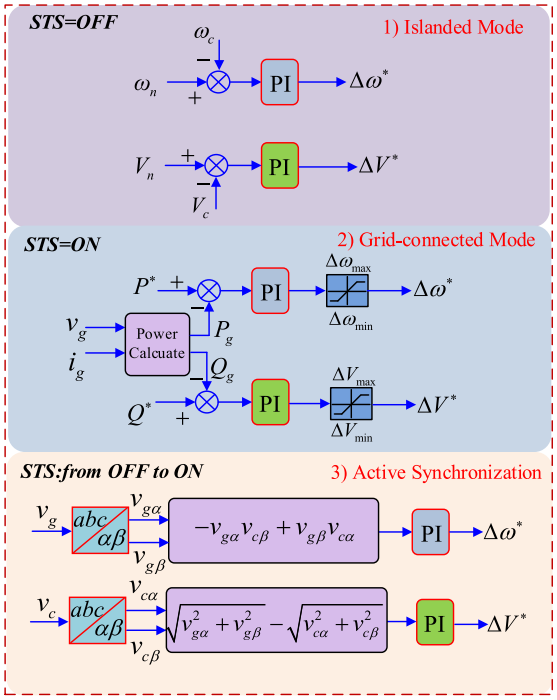

FIGURE 7. The mode-supervisory controller.

C. TERTIARY MODE-SUPERVISORY CONTROL

The tertiary mode-supervisory control aims to manage different operation modes and prescribe the compensation signals $\Delta\omega^*$, ΔV^* for secondary control of leader DGs. As shown in Fig. 7, mode-supervisory controller is meant to automatically select the different input signals according to the status of the STS (1 means ON; 0 means OFF):

1) STS = 0 when microgrid works in islanded (IS) mode;
2) STS = 1 when microgrid works in grid-connected (GC) mode;
3) STS switches from 1 to 0 when microgrid works mode transition from GC mode to IS mode by disconnecting microgrid with utility-grid due to the grid fault;
4) STS switches from 0 to 1 when active synchronization control is activated by reconnecting microgrid back to utility-grid after fault clearing.

- *Control Compensation Signals $\Delta\omega^*$, ΔV^* in IS Mode*

In IS mode, the compensation signals $\Delta\omega^*$ and ΔV^* are set as follows in order to restore the voltage/frequency amplitudes

$$\begin{cases} \Delta\omega^* = (k_{p\omega 1} + \dfrac{k_{i\omega 1}}{s})(\omega_n - \omega_c) \\ \Delta V^* = (k_{pv1} + \dfrac{k_{iv1}}{s})(V_n - V_c) \end{cases} \tag{7}$$

where ω_c and V_c are the angular-frequency and voltage-amplitude of PCC. ω_n and V_n are system nominal angular-frequency and voltage references. $k_{p\omega 1}$ and $k_{i\omega 1}$ are

proportional-integral (PI) coefficients of frequency-recovery control. k_{pv1} and k_{iv1} are PI coefficients of voltage-recovery control.

- *Control Compensation Signals $\Delta\omega^*$, ΔV^* in GC Mode*

In GC mode, to flexible management the grid-injected active/reactive power, the control compensation signals $\Delta\omega^*$ and ΔV^* are designed

$$\begin{cases} \Delta\omega^* = (k_{p\omega 2} + \dfrac{k_{i\omega 2}}{s})(P^* - P_g) \\ \Delta V^* = (k_{pv2} + \dfrac{k_{iv2}}{s})\left(Q^* - Q_g\right) \end{cases} \tag{8}$$

where P_g and Q_g are the calculated active and reactive power injected into utility-grid in real-time. P^* and Q^* are the grid-injected active and reactive power references. $k_{p\omega 2}$ and $k_{i\omega 2}$ are PI coefficients of active power control. k_{pv2} and k_{iv2} are PI coefficients of reactive power control.

- *Control Compensation Signals $\Delta\omega^*$, ΔV^* in AS Mode*

In the active synchronization (AS) from IS mode to GC mode, for the purpose of seamless transition, PCC should synchronize with utility-grid in voltage-amplitude, frequency and phase. Thus, the active synchronization compensation signals $\Delta\omega^*$ and ΔV^* are given

$$\begin{cases} \Delta\omega^* = (k_{p\omega 3} + \dfrac{k_{i\omega 3}}{s})(-v_{g\alpha}v_{c\beta} + v_{g\beta}v_{c\alpha}) \\ \quad\quad = (k_{p\omega 3} + \frac{k_{i\omega 3}}{s})V_cV_g\sin(\delta_g - \delta_c) \\ \Delta V^* = (k_{pv3} + \dfrac{k_{iv3}}{s})\left(\sqrt{v_{g\alpha}^2 + v_{g\beta}^2} - \sqrt{v_{c\alpha}^2 + v_{c\beta}^2}\right) \\ \quad\quad = (k_{pv3} + \frac{k_{iv3}}{s})(V_g - V_c) \end{cases} \tag{9}$$

where $v_{g\alpha}$ and $v_{g\beta}$ are the direct-/quadrature-axis voltage components of utility-grid. V_g and δ_g are the voltage amplitude and phase of utility-grid. $v_{c\alpha}$ and $v_{c\beta}$ are the direct-/quadrature-axis voltage components of PCC. V_c and δ_c are the voltage amplitude and phase of PCC. $k_{p\omega 3}$ and $k_{i\omega 3}$ are PI coefficients of voltage-phase pre-synchronization control. k_{pv3} and k_{iv3} are PI coefficients of voltage-amplitude pre-synchronization control.

It is worth noting that all control compensation signals $\Delta\omega^*$ and ΔV^* are derived by PI controllers, which are slow-dynamic averaged values. In this way, these two DC components can only change within a small range in several switching cycles [27], and then can be sent from the mode-supervisory controller to the leader DGs via a low bandwidth communication. The execution speed can reach at 5 Mb/s with optical fiber [38].

IV. STABILITY ANALYSIS

To discuss the system stability and design control parameters of distributed hierarchical control, a small signal model is built, and eigenvalue analysis is carried out in this section. Generally, the line impedance is mainly inductive [15]. Thus, the delivered active-power depends mostly on the power-angle, and reactive-power is predominately dependent on voltage-amplitude-difference. Thus, stability analysis of P-ω and Q-V can be decoupled to facilitate their individual designs [36], [37].

A. POWER ANGLE STABILITY ANALYSIS

1) OVERALL SYSTEM MODEL OF P-ω CONTROL

Typically, for multiple-parallel DGs connected to PCC, their frequency control dynamics are obtained from (3)

$$\begin{cases} \dot{\delta}_1 = \omega^* - m_1P_1 + \Delta\omega_1 \\ \dot{\delta}_2 = \omega^* - m_2P_2 + \Delta\omega_2 \\ \quad\quad\vdots \\ \dot{\delta}_n = \omega^* - m_nP_n + \Delta\omega_n \end{cases} \tag{10}$$

where the delivered active power is calculated as [15]

$$P_i = \frac{V_iV_c}{X_i}\sin(\delta_i - \delta_c) \tag{11}$$

$$\dot{\delta}_i = \omega_i \quad (i = 1, 2\cdots n) \tag{12}$$

where V_i and δ_i are output voltage-amplitude and angle of DG-i. V_c and δ_c are voltage-amplitude and angle of PCC. X_i is the linking reactance between i-th DG and PCC.

In (10), $\Delta\omega_i$ is presented as follows from (4)

$$\begin{cases} \Delta\omega_1 = \dfrac{1}{k_\omega}\displaystyle\int\sum a_{1j}\left(\Delta\omega_j - \Delta\omega_1\right)dt \\ \qquad\quad + \dfrac{1}{k_\omega}\displaystyle\int\gamma_1\left(\Delta\omega^* - \Delta\omega_1\right)dt \\ \Delta\omega_2 = \dfrac{1}{k_\omega}\displaystyle\int\sum a_{2j}\left(\Delta\omega_j - \Delta\omega_2\right)dt \\ \qquad\quad + \dfrac{1}{k_\omega}\displaystyle\int\gamma_2\left(\Delta\omega^* - \Delta\omega_2\right)dt \\ \qquad\quad\vdots \\ \Delta\omega_n = \dfrac{1}{k_\omega}\displaystyle\int\sum a_{nj}\left(\Delta\omega_j - \Delta\omega_n\right)dt \\ \qquad\quad + \dfrac{1}{k_\omega}\displaystyle\int\gamma_n\left(\Delta\omega^* - \Delta\omega_n\right)dt \end{cases} \tag{13}$$

where $\Delta\omega^*$ is the control compensation signal, derived from the tertiary mode-supervisory controller (7)-(9)

$$\Delta\omega^* = \begin{cases} (k_{p\omega 1} + \dfrac{k_{i\omega 1}}{s})(\omega_n - \omega_c); & \text{In IS mode} \\ (k_{p\omega 2} + \dfrac{k_{i\omega 2}}{s})(P^* - P_g); & \text{In GC mode} \\ (k_{p\omega 3} + \dfrac{k_{i\omega 3}}{s})V_cV_g\sin(\delta_g - \delta_c); & \text{In AS mode} \end{cases} \tag{14}$$

where

$$P^* - P_g = \frac{V_gV_c}{X_g}[\sin(\delta_c^* - \delta_g) - \sin(\delta_c - \delta_g)] \tag{15}$$

where V_g, δ_g, ω_g are the voltage-amplitude, angle and angular frequency of utility-grid. X_g is the grid reactance between PCC and utility-grid. δ_c^* is the nominal voltage angle reference of PCC in the grid-connected mode.

In addition, according to the system constraint of supply-demand power balance, (16) is presented

$$P_1 + P_2 + \cdots + P_n = P_L \tag{16}$$

where P_L implies an active power value of total load demand.

2) LINEARIZATION OF OVERALL SYSTEM MODEL

As the power angle $|\delta_n - \delta_c|_\infty$ is always small in microgrid, $\sin(\delta_n - \delta_c) \cong (\delta_n - \delta_c)$ and $\cos(\delta_n - \delta_c) \cong 1$. Then, the linearization of overall system model is conducted.

a: LINEARIZATION OF PRIMARY DROOP CONTROL (10)

$$\dot{\tilde{\delta}} = -K\left(\tilde{\delta} - \tilde{\delta}_c\eta\right) + \Delta\tilde{\omega} \tag{17}$$

where

$$\begin{cases} \tilde{\delta} = \begin{bmatrix} \tilde{\delta}_1 & \tilde{\delta}_2 & \cdots & \tilde{\delta}_n \end{bmatrix}^T; \quad \eta = \begin{bmatrix} 1 & 1 & \cdots & 1 \end{bmatrix}^T \\ \Delta\tilde{\omega} = \begin{bmatrix} \Delta\tilde{\omega}_1 & \Delta\tilde{\omega}_2 & \cdots & \Delta\tilde{\omega}_n \end{bmatrix}^T \\ K = diag[\, m_1k_1 \quad m_2k_2 \quad \cdots \quad m_nk_n \,] \\ k_i = \dfrac{V_iV_c}{X_i}\cos(\delta_i - \delta_c) \end{cases} \tag{18}$$

b: LINEARIZATION OF SECONDARY DISTRIBUTED CONTROL (13)

$$\Delta\dot{\tilde{\omega}} = -L\Delta\tilde{\omega} + \gamma\left(\Delta\tilde{\omega}^*\eta - \Delta\tilde{\omega}\right) \tag{19}$$

where

$$\begin{cases} L = \dfrac{1}{k_\omega}\begin{bmatrix} \sum a_{1i} & -a_{12} & \cdots & -a_{1n} \\ -a_{21} & \sum a_{2i} & \cdots & -a_{2n} \\ \vdots & \vdots & \ddots & \vdots \\ -a_{n1} & -a_{n2} & \cdots & \sum a_{nn} \end{bmatrix} \\ \gamma = \dfrac{1}{k_\omega}diag[\, \gamma_1 \quad \gamma_2 \quad \cdots \quad \gamma_n \,] \end{cases} \tag{20}$$

c: LINEARIZATION OF TERTIARY CONTROL (14)-(15)

$$\Delta\dot{\tilde{\omega}}^* = \begin{cases} (k_{p\omega 1} + \dfrac{k_{i\omega 1}}{s})(\dot{\omega}_g - \ddot{\tilde{\delta}}_c); & \text{In IS mode} \\ (k_{p\omega 2} + \dfrac{k_{i\omega 2}}{s})\dfrac{V_gV_c}{X_g}(\omega_g - \dot{\tilde{\delta}}_c); & \text{In GC mode} \\ (k_{p\omega 3} + \dfrac{k_{i\omega 3}}{s})V_cV_g(\omega_g - \dot{\tilde{\delta}}_c); & \text{In AS mode} \end{cases} \tag{21}$$

From (21), a unified form of $\Delta\omega^*$ is obtained for both GC mode and AS mode

$$\Delta\dot{\tilde{\omega}}^* = (k_{p\omega} + \frac{k_{i\omega}}{s})(\omega_g - \dot{\tilde{\delta}}_c)\text{In GC \& AS modes} \tag{22}$$

where

$$k_{p\omega} = \frac{V_gV_c}{X_g}k_{p\omega 2} = V_cV_gk_{p\omega 3};\ k_{i\omega} = \frac{V_gV_c}{X_g}k_{i\omega 2} = V_cV_gk_{i\omega 3} \tag{23}$$

For simplicity, only the stability analysis of GC and AS modes (22) is carried out here. The similar analysis can be also applied to IS mode in (21).

d: LINEARIZATION OF SYSTEM CONSTRAINT (16)

$$k_1\left(\tilde{\delta}_1 - \tilde{\delta}_c\right) + \cdots + k_n\left(\tilde{\delta}_n - \tilde{\delta}_c\right) = 0 \tag{24}$$

e: SYSTEM STATE SPACE MODEL OF P-ω CONTROL

For the tracking phase synchronization, a new state variable $\tilde{\theta}$ is set to facilitate the stability analysis.

$$\tilde{\theta} = \tilde{\delta} - (\omega_g t)\eta \tag{25}$$

The system linearization is given by combining (17)-(24)

$$\begin{cases} \dot{\tilde{\theta}} = -K_1\tilde{\theta} + \Delta\tilde{\omega} - \omega_g\eta \\ \Delta\dot{\tilde{\omega}} = -L\Delta\tilde{\omega} + \gamma\left(\Delta\tilde{\omega}^*\eta - \Delta\tilde{\omega}\right) \\ \Delta\dot{\tilde{\omega}}^* = (\dfrac{k_{p\omega}}{k_{tol}}K_2K_1 - \dfrac{k_{i\omega}}{k_{tol}}K_2)\tilde{\theta} - \dfrac{k_{p\omega}}{k_{tol}}K_2(\Delta\tilde{\omega} - \omega_g\eta) \end{cases} \tag{26}$$

where

$$\begin{cases} k_{tol} = \sum_{i=1}^{n} k_i \\ K_2 = \begin{bmatrix} k_1 & k_2 & \cdots & k_n \end{bmatrix} \\ K_1 = K - \dfrac{1}{k_{tol}}\begin{bmatrix} m_1k_1 & m_2k_2 & \cdots & m_nk_n \end{bmatrix}^T \begin{bmatrix} k_1 & k_2 & \cdots & k_n \end{bmatrix} \end{cases} \tag{27}$$

The state-space equations of the power angle stability is presented as

$$\dot{\tilde{X}}_\omega = [A_\omega]\tilde{X}_\omega \tag{28}$$

where

$$\tilde{X}_\omega = \begin{bmatrix} \tilde{\theta}_{n\times 1} \\ \Delta\tilde{\omega}_{n\times 1} \\ \Delta\tilde{\omega}^* \end{bmatrix} \tag{29}$$

$$A_\omega = \left[\begin{array}{ccc:ccc:c} & & & & & & 0 \\ & -(K_1)_{n\times n} & & & I_{n\times n} & & \vdots \\ & & & & & & 0 \\ \hdashline & & & & & & \gamma_1 \\ & 0_{n\times n} & & & -(L+\gamma)_{n\times n} & & \vdots \\ & & & & & & \gamma_n \\ \hdashline A_1 & \cdots & A_n & \frac{k_{p\omega}k_1}{k_{tol}} & \cdots & \frac{k_{p\omega}k_n}{k_{tol}} & 0 \end{array}\right] \tag{30}$$

where

$$A_n = \frac{k_n}{k_{tol}}\{k_{p\omega}[m_nk_n - \frac{\sum m_nk_n^2}{k_{tol}}] - k_{i\omega}\} \tag{31}$$

3) EIGENVALUE ANALYSIS OF A_ω

To test the stability of the proposed active power-frequency control scheme, the eigenvalues analysis of matrix A_ω is applied. According to the simulation system described in Section V, the root-locus plots is studied by varying the secondary control gain k_ω of (4) and tertiary PI control coefficients $k_{p\omega}$, $k_{i\omega}$ of (23).

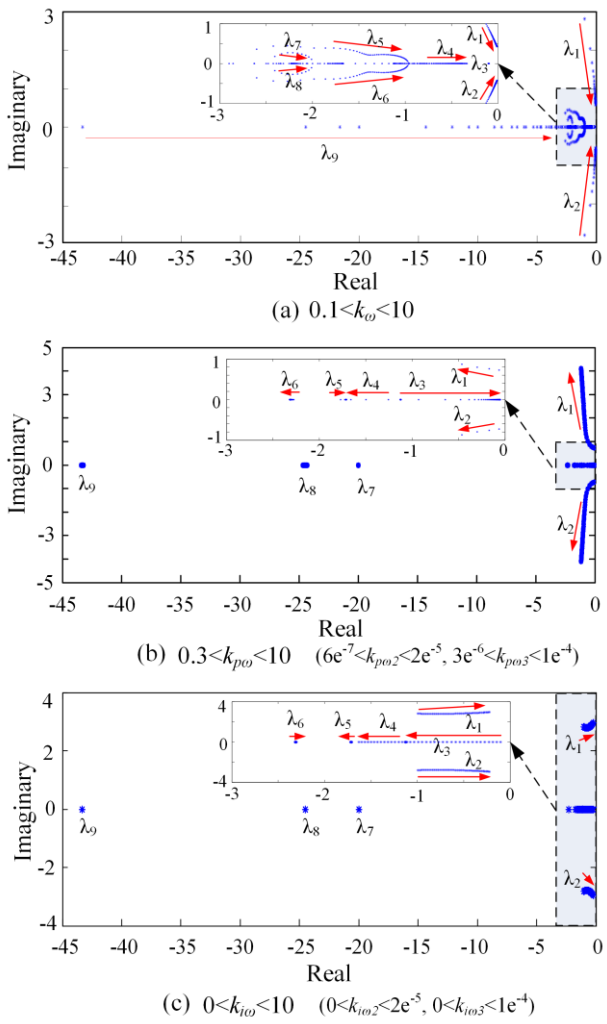

FIGURE 8. Root locus of system matrix A_ω. (a) $0.1 < k_\omega < 10$, (b) $0.3 < k_{p\omega} < 10$, (c) $0 < k_{i\omega} < 10$.

Fig. 8(a) shows the root locus diagram as k_ω increases from 0.1 to 10. As seen, the poles λ_1 and λ_2 are gradually moved to the imaginary axis, which might lead to a poor dynamic response and even instability. Therefore, k_ω should choose a relatively small value.

Fig. 8(b) depicts the root locus diagram as $k_{p\omega}$ increases from 0.3 to 10. From (23), it also means $6e^{-7} < k_{p\omega2} < 2e^{-5}$ and $3e^{-6} < k_{p\omega3} < 1e^{-4}$. When $k_{p\omega}$ is small, λ_1 and λ_2 is the dominant poles. With increasing $k_{p\omega}$, λ_1 and λ_2 move away from the imaginary axis, and λ_3 moves close to the imaginary axis. To obtain a fine damping ratio of the system, $k_{p\omega} = 5$ is set in the simulation.

Fig. 8(c) presents the root locus diagram as $k_{i\omega}$ increases from 0 to 10. From (23), it also means $0 < k_{i\omega2} < 2e^{-5}$ and $0 < k_{i\omega3} < 1e^{-4}$. When $k_{i\omega}$ increases, λ_1 and λ_2 turn into the dominant complex conjugate poles, resulting in a second-order dynamic behavior. However, a too large $k_{i\omega}$ would make the system easy to be unstable. Thus, $k_{i\omega} = 0.5$ is set in the simulation.

B. VOLTAGE STABILITY ANALYSIS

1) OVERALL SYSTEM MODEL OF Q-V CONTROL

For multiple DGs connected to PCC, their Q-V control dynamics are obtained from (5)

$$\begin{cases} V_1 = V^* - n_1 Q_1 + \Delta V_1 + \beta_1 \Delta V^* \\ V_2 = V^* - n_2 Q_2 + \Delta V_2 + \beta_2 \Delta V^* \\ \vdots \\ V_n = V^* - n_n Q_n + \Delta V_n + \beta_n \Delta V^* \end{cases} \tag{32}$$

where

$$Q_i = \frac{V_i (V_i - V_c)}{X_i} \tag{33}$$

where V_i and V_c are the voltage amplitudes of i-th DG and PCC.

In (32), ΔV_i is presented as follows from (6)

$$\begin{cases} \Delta V_1 = \dfrac{1}{k_v} \int \sum b_{1j} \left(k_{Qj} Q_j - k_{Q1} Q_1 \right) dt \\ \Delta V_2 = \dfrac{1}{k_v} \int \sum b_{2j} \left(k_{Qj} Q_j - k_{Q2} Q_2 \right) dt \\ \vdots \\ \Delta V_n = \dfrac{1}{k_v} \int \sum b_{nj} \left(k_{Qj} Q_j - k_{Qn} Q_n \right) dt \end{cases} \tag{34}$$

In (32), ΔV^* is the voltage control compensation signal, derived from the tertiary mode-supervisory controller (7)-(9)

$$\Delta V^* = \begin{cases} (k_{pv1} + \dfrac{k_{iv1}}{s})(V_n - V_c); & \text{In IS mode} \\ (k_{pv2} + \dfrac{k_{iv2}}{s})(Q^* - Q_g); & \text{In GC mode} \\ (k_{pv3} + \dfrac{k_{iv3}}{s})(V_g - V_c); & \text{In AS mode} \end{cases} \tag{35}$$

where

$$Q^* - Q_g = \frac{V_c^* \left(V_c^* - V_g \right)}{X_g} - \frac{V_c \left(V_c - V_g \right)}{X_g} \tag{36}$$

where V_c^* is the nominal voltage amplitude reference of PCC in GC mode.

Moreover, according to the system constraint of supply-demand power balance, (37) is presented

$$Q_1 + Q_2 + \cdots + Q_n = Q_L \tag{37}$$

where Q_L implies a reactive power value of total load demand.

2) LINEARIZATION OF OVERALL SYSTEM MODEL

a: LINEARIZATION OF PRIMARY DROOP CONTROL (32)-(33)

$$\tilde{V} = -N\tilde{Q} + \Delta\tilde{V} + \beta\Delta\tilde{V}^* \tag{38}$$

$$\tilde{Q} = C_{diag}\tilde{V} - D\tilde{V}_c \tag{39}$$

where

$$\begin{cases} \tilde{V} = [\,\tilde{V}_1 \quad \tilde{V}_2 \quad \cdots \quad \tilde{V}_n\,]^T; \\ \Delta\tilde{V} = [\,\Delta\tilde{V}_1 \quad \Delta\tilde{V}_2 \quad \cdots \quad \Delta\tilde{V}_n\,]^T \\ N = diag[\,n_1 \quad n_2 \quad \cdots \quad n_n\,]; \\ \tilde{Q} = [\,\tilde{Q}_1 \quad \tilde{Q}_2 \quad \cdots \quad \tilde{Q}_n\,]^T \\ \beta = [\,\beta_1 \quad \beta_2 \quad \cdots \quad \beta_n\,]^T \\ C_{diag} = diag[\,c_1 \quad c_2 \quad \cdots \quad c_n\,]; \quad c_i = \dfrac{2V_i - V_c}{X_i} \\ D = [\,d_1 \quad d_2 \quad \cdots \quad d_n\,]^T; \quad d_i = \dfrac{V_i}{X_i} \end{cases} \tag{40}$$

b: LINEARIZATION OF SECONDARY DISTRIBUTED CONTROL (34)

$$\Delta\dot{\tilde{V}} = -L_V K_Q \tilde{Q} \tag{41}$$

where

$$\begin{cases} L_V = \dfrac{1}{k_v}\begin{bmatrix} \sum b_{1i} & -b_{12} & \cdots & -b_{1n} \\ -b_{21} & \sum b_{2i} & \cdots & -b_{2n} \\ \vdots & \vdots & \ddots & \vdots \\ -b_{n1} & -b_{n2} & \cdots & \sum b_{nn} \end{bmatrix} \\ K_Q = diag[\,k_{Q1} \quad k_{Q2} \quad \cdots \quad k_{Qn}\,] \end{cases} \tag{42}$$

c: LINEARIZATION OF TERTIARY MODE-SUPERVISORY CONTROL (35)-(36)

$$\Delta\tilde{V}^* = \begin{cases} (k_{pv1} + \dfrac{k_{iv1}}{s})(-\tilde{V}_c); & \text{In IS mode} \\ (k_{pv2} + \dfrac{k_{iv2}}{s})c_c(-\tilde{V}_c); & \text{In GC mode} \\ (k_{pv3} + \dfrac{k_{iv3}}{s})(-\tilde{V}_c); & \text{In AS mode} \end{cases} \tag{43}$$

where

$$c_c = \frac{2V_c - V_g}{X_g} \tag{44}$$

From (21), a unified form of ΔV^* is obtained for IS mode, GC mode, and AS mode

$$\Delta\tilde{V}^* = (k_{pv} + \frac{k_{iv}}{s})(-\tilde{V}_c) \tag{45}$$

where

$$k_{pv} = k_{pv1} = c_c k_{pv2} = k_{pv3}; \quad k_{iv} = k_{iv1} = c_c k_{iv2} = k_{iv3} \tag{46}$$

d: LINEARIZATION OF SYSTEM CONSTRAINT (37)

$$c_1\tilde{V}_1 - d_1\tilde{V}_c + c_2\tilde{V}_2 - d_2\tilde{V}_c + \cdots + c_n\tilde{V}_n - d_n\tilde{V}_c = 0 \tag{47}$$

Then,

$$\tilde{V}_c = \frac{\sum c_i\tilde{V}_i}{\sum d_i} = \frac{1}{d_{tol}} C\tilde{V} \tag{48}$$

where

$$C = [\,c_1 \quad c_2 \quad \cdots \quad c_n\,]; \quad d_{tol} = \sum_{i=1}^{n} d_i \tag{49}$$

e: SYSTEM STATE-SPACE OF Q-V CONTROL

The entire system linearization is given from (38)-(49)

$$\dot{\tilde{X}}_V = [A_V]\tilde{X}_V \tag{50}$$

In this study, given

$$\tilde{X}_V = \left[\tilde{V}\right]_{n\times 1} \tag{51}$$

$$A_V = -FL_V K_Q E - \frac{k_{iv}}{d_{tol}} F\beta C \tag{52}$$

where

$$E = C_{diag} - \frac{DC}{d_{tol}}; F = \left[I + NE + \frac{k_{pv}}{d_{tol}}\beta C\right]^{-1} \tag{53}$$

3) EIGENVALUE ANALYSIS OF A_V

To test the stability of the proposed Q-V control scheme, the eigenvalues analysis of matrix A_V is applied. According to the simulation system in Section V, the root-locus plots is studied in Fig.9 by varying the secondary control gain k_v of (6) and tertiary PI control coefficients k_{pv}, k_{iv} of (46).

Fig. 9 shows that the system dominant pole λ_1 is mainly affected by k_{pv} and k_{iv} in Fig. 9(b)-(c). With increasing k_{pv}, λ_1 move close to the imaginary axis. On the contrary, increasing k_{iv} make λ_1 move away from the imaginary axis. To guarantee a satisfactory dynamic response, k_{pv} should choose a relatively small value, and k_{iv} should choose a relatively large value. In the simulation, $k_v = 0.01$, $k_{pv} = 2$ and $k_{iv} = 1$ are set by consideration of the system dynamic stability. Then, k_{pv1}, k_{pv2}, k_{pv3} and k_{iv1}, k_{iv2}, k_{iv3} are derived from the equivalence relation in (46).

V. SIMULATION RESULTS

The proposed distributed hierarchical control is verified with time-domain simulations. The simulation-parameters are listed in Table I. The overall control scheme is shown in Fig. 3. The simulated model in Fig.10 is a typical radial 4-buses/4-DGs microgrid configuration, which has been widely performed in microgrid case study [26]-[33]. Therefore, this configuration can represent the multi-buses/multi-DGs microgrid system. The system includes four inverter-based DGs (DG1∼DG4), four independent local loads ($L_1 \sim L_4$) and a public load L_0. DG1 is chosen as the leader-DG and acquires control compensation signals from the mode-supervisory controller. DG2∼DG3 are the follower DGs. From Fig. 10, the associated adjacency matrices $A = [a_{ij}]$ and $B = [b_{ij}]$ are given

$$A = \begin{pmatrix} 0 & 1 & 0 & 1 \\ 1 & 0 & 1 & 0 \\ 0 & 1 & 0 & 1 \\ 1 & 0 & 1 & 0 \end{pmatrix}, \quad B = \begin{pmatrix} 0 & 0 & 0 & 0 \\ 1 & 0 & 1 & 0 \\ 0 & 1 & 0 & 1 \\ 1 & 0 & 1 & 0 \end{pmatrix} \tag{54}$$

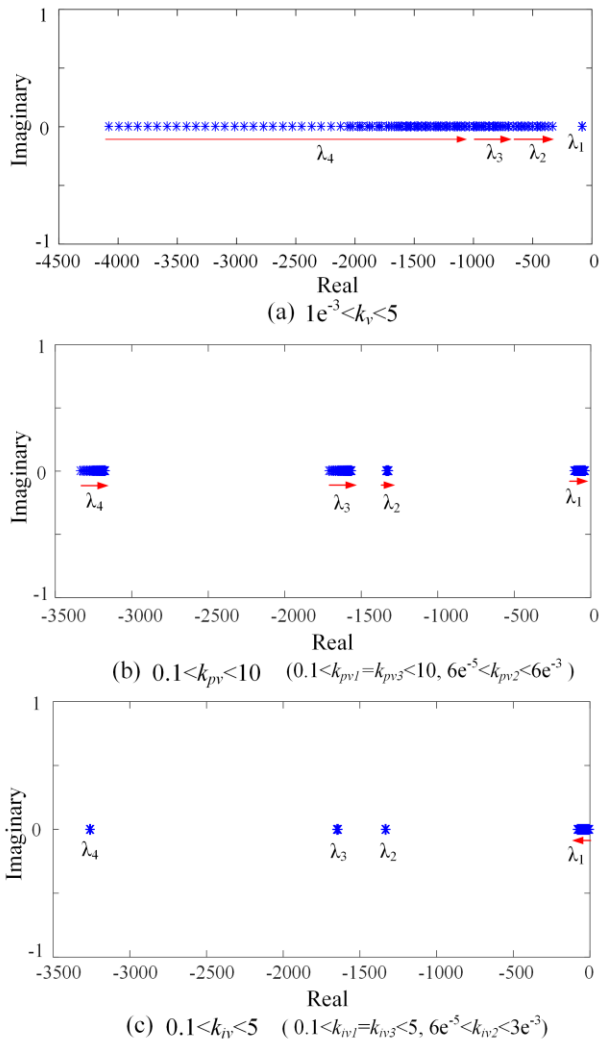

FIGURE 9. Root locus of system matrix A_V . (a) $1e^{-3} < k_v < 5$, (b) $0.1 < k_{pv} < 10$, (c) $0.1 < k_{iv} < 5$.

A. CASE-1: SEAMLESS TRANSITION FROM GC MODE TO IS MODE

This case performs the simulation from GC mode to IS mode under the distributed hierarchical control. Fig. 11 and Fig. 12 show the simulation results of case-1. Before t = 1s, the microgrid operates in GC mode normally. At t = 1s, the STS switches from ON to OFF due to the grid fault, and the microgrid disconnects with utility-grid. After t = 1s, the microgrid works mode transition from GC mode to IS mode, and the tertiary mode-supervisory controller automatically switches to the islanded-mode input signal.

From Fig. 11(a)-(b), the injected active and reactive power into the utility-grid are $P_g = P^* = 10$ kW and $Q_g = Q^* = 3$ kVar at the beginning of GC mode. After t = 1s, the islanded microgrid is formed ($P_g = 0$ kW and $Q_g = 0$ kVar). In IS mode, Fig. 11(d) and Fig. 11(f) reveal that a nominal system operation frequency ($f_c = 50$ Hz) and rated voltage amplitude of PCC ($V_c = 311$ V) are guaranteed

TABLE 1. Simulation parameters.

Parameter	*Symbol*	*Value*
Electrical parameters		
Nominal voltage	V_n	311 V
Nominal frequency	f_n	50 Hz
Line impedance	Z_{01}	0.8+j1.0 Ω
Line impedance	Z_{02}	1.6+j2.0 Ω
Line impedance	Z_{23}	0.9+j1.2 Ω
Line impedance	Z_{04}	1.2+j1.5 Ω
Grid impedance	X_g	j0.2 Ω
Loads L_1=L_2=L_3=L_4		P=2 kW, Q=2 kVar
Load L_0		P=4 kW, Q=3 kVar
Primary Droop Control Parameters		
P-ω droop coefficient	m_i	10^{-5}
Q-V droop coefficient	n_i	10^{-3}
Distributed control Parameters		
Frequency control gain	k_ω	0.1
Voltage control gain	k_v	0.01
Tertiary PI Control Parameters		
Rated grid-injected active power	P^*	10 kW
Rated grid-injected reactive power	Q^*	3 kVar
Frequency proportional term	$k_{p\omega}$	5
Frequency integral term	$k_{i\omega}$	0.5
Voltage proportional term	k_{pv}	2
Voltage integral term	k_{iv}	1

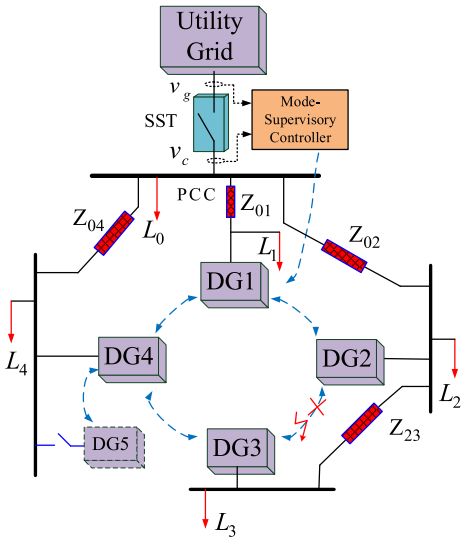

FIGURE 10. Simulated microgrid physical and communication models.

in steady-state. Moreover, Fig. 11(c) presents the grid-injected current, and Fig. 11(e) gives the instantaneous voltage of PCC during t = 0.6s∼1.4s.

Fig. 12 show simulation results of four-DGs. From Fig. 12(a)-(b), DG1∼DG4 have a satisfied voltage and frequency transition process, and realizes a seamless transition from GC mode to IS mode after several cycles. Moreover, as seen in Fig. 12(c)-(d), four DGs have an accurate load power sharing whether in GC mode or IS mode.

In case-1, the proposed distributed hierarchical control achieves all the required performances and control targets under GC mode, IS mode and mode transition from GC mode to IS mode.

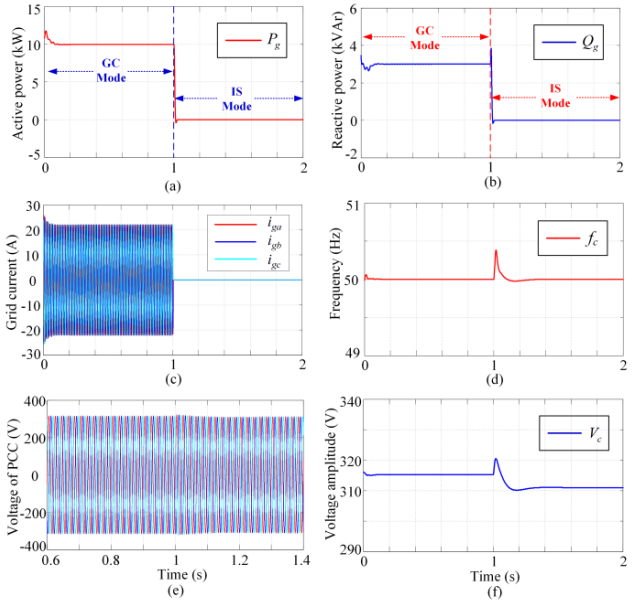

FIGURE 11. Results in case-1: (a) active-power-injected grid, (b) reactive-power-injected grid, (c) grid current, (d) PCC frequency, (e) instantaneous PCC voltage, (f) PCC voltage amplitude.

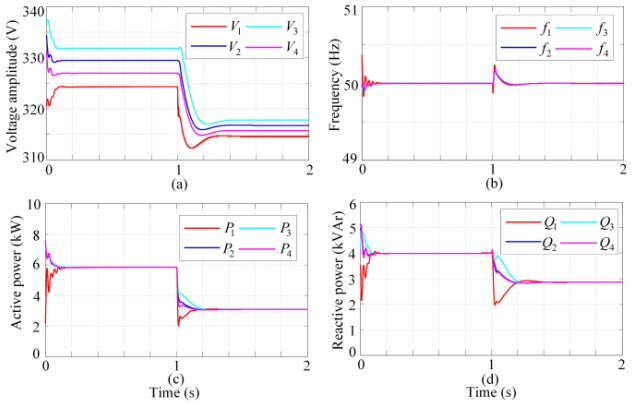

FIGURE 12. Results of four DGs in case-1: (a) voltage-amplitudes, (b) frequencies, (c) output active-power, (d) output reactive-power.

B. CASE-2:ACTIVE SYNCHRONIZATION FROM IS MODE TO GC MODE

In case-2, the proposed distributed hierarchical control scheme is validated during the active synchronization (AS) from IS mode to GC mode. Fig. 13 shows the simulation results of case-2.

Initially, microgrid disconnects with the utility-grid and works in islanded mode. Meanwhile, the tertiary mode-supervisory controller chooses the control input signals of islanded mode.

At t = 1s, active synchronization control is activated after grid-fault clearing, and the tertiary mode-supervisory controller automatically switches to the control input signals of active synchronization.

After few seconds, the frequency error between grid and PCC in Fig. 13(f), phase angle error in Fig. 13(g), and amplitude difference in Fig. 13(d) meet the microgrid

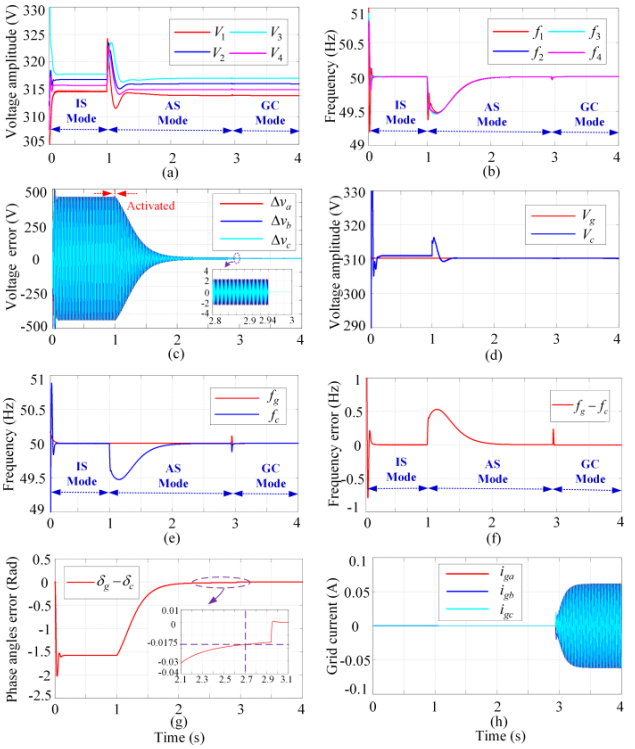

FIGURE 13. Results in case-2: (a) DGs voltage amplitudes, (b) DGs frequencies, (c) voltage difference between grid and PCC, (d) voltage amplitudes of grid and PCC, (e) frequencies of grid and PCC, (f) difference of frequency, (g) difference of phase angle, (h) grid current.

synchronization criterion [23] at t = 2.7s, and STS switches from OFF to ON. The microgrid is reconnected to utility-grid in GC mode.

As seen in Fig. 13(c), when active synchronization control is activated, the voltage differences Δv between PCC and grid decreases rapidly. At t = 2.7s when the voltage of PCC meet the synchronization criteria, the instantaneous voltage difference would be almost zero. After closing STS, the instantaneous grid currents in Fig. 13(h) are very small and mostly no current inrush. Thus, a seamless active synchronization is attained. Moreover, Fig. 13(a) and Fig. 13(b) reveal that output voltage-amplitudes and frequencies of four DGs always lie in the permissible ranges during the mode transition from IS mode to GC mode, which verifies the effectiveness of the proposed distributed hierarchical control framework.

C. CASE-3:COMMUNICATION-LINK-FAILURE RESILIENCY IN ACTIVE SYNCHRONIZATION MODE

Resiliency to a single communication-link-failure is considered in active synchronization mode as shown in Fig. 14. Compared with case-2, the simulation process is similar while the communication link between DG2 and DG3 fails in Fig. 10. As there is also a spanning tree between each DG and the tertiary mode-supervisory controller after one link 2-3 failure, the proposed distributed hierarchical control can remain operational. As seen in Fig. 14, the link 2-3 failure

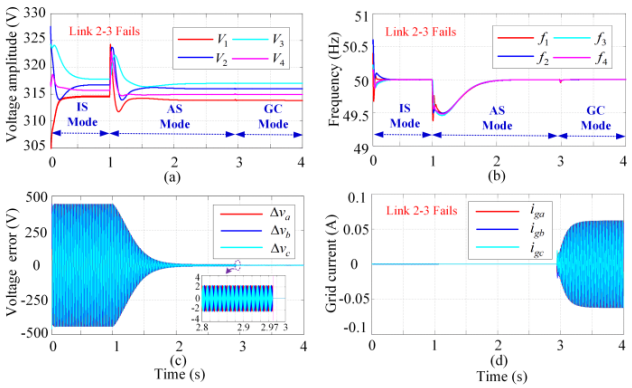

FIGURE 14. Results in case-3: (a) DGs voltage amplitudes, (b) DGs frequencies, (c) voltage difference between grid and PCC, (d) grid current.

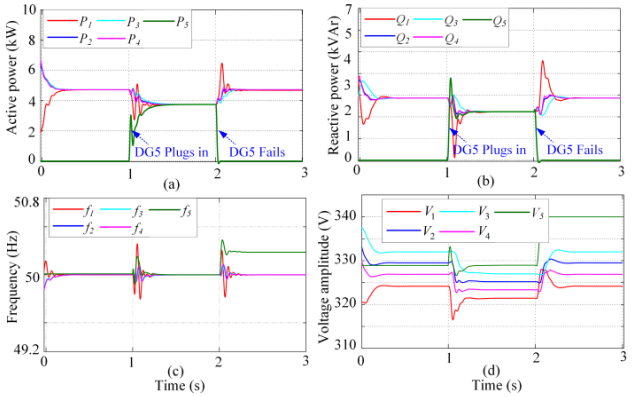

FIGURE 15. Results of five DGs in case-4: (a) output active-power, (b) output reactive-power, (c) frequencies, (d) voltage-amplitudes.

does not impact on seamless transition from IS mode to GC mode, and a satisfactory performance is guaranteed. It should be noted that the reconfiguration caused by the link-failure just affects the Laplacian matrix and dynamic response but not the steady-state performances.

In contrast, any link-failure of the central-standard hierarchical control [26], [27] would break off the information flow and turn the whole microgrid system abnormal. Thus, the centralized-star-communication network is risk subjected to the failure of a single point, which limits its application on a practical multi-bus microgrid. Alternatively, the proposed distributed hierarchical control overcomes the failure of single point with a sparse distributed communication network. Thus, the proposed method has higher communication reliability than the central-standard hierarchical control [26], [27].

D. CASE-4: PLUG-AND-PLAY CAPABILITY IN GC MODE

The proposed distributed hierarchical control scheme can accommodate a plug-and-play and scalability environment so that new DG can be augmented to the system. Fig. 15 shows the performance when DG5 plugs at t = 1s and fails at t = 2s, connected in bus-4 of Fig. 10. The DG5 gets the communication signal from DG4, and the new graph still has a spanning tree. Meanwhile, as the tertiary mode-supervisory controller was already pinning to DG4 of the old graph before adding DG5, there is not necessary for the tertiary controller to directly pin to DG5.

As seen, DG5 becomes automatically synchronized with the existing DG1∼DG4 in Fig. 15(c), and the accurate power sharing has been updated in Fig. 15(a)-(b) when DG5 comes into the system. Then, if DG5 fails at t = 2s, DG5 can be disconnected from the rest system, and the remaining control system is still functional. The proposed distributed hierarchical control also readjusts the power sharing among the remaining DG1∼DG4. Simultaneously, the output voltage amplitudes are also regulated accordingly in Fig. 15(d).

VI. CONCLUSIONS

This study introduces a distributed hierarchical control for AC microgrid taking consideration of all the practical operation modes. It can operate in both grid-connected modes, islanded mode and seamless transition modes between them. The proposed control combines the primary droop control, secondary distributed leader-follower control, and tertiary mode-supervisory control. Only few leader DGs near the PCC acquire the compensation signals from the top-level mode-supervisory controller. The rest follower DGs would follow leader-DGs, and exchange information with their neighbors by the distributed consensus protocol. Finally, all DGs reach an agreement and fulfill group targets in different operation modes. On the whole, all main control targets are achieved, and this systematic hierarchical control frame provides a cost-effective method for a practical microgrid.

REFERENCES

[1] R. H. Lasseter, "MicroGrids," in *Proc. IEEE Power Eng. Soc. Winter Meeting*, 2002, pp. 305–308.

[2] K. Shi, H. Ye, W. Song, and G. Zhou, "Virtual inertia control strategy in microgrid based on virtual synchronous generator technology," *IEEE Access*, vol. 6, pp. 27949–27957, 2018, doi: 10.1109/ACCESS.2018.2839737.

[3] H. Jia, Q. Xiao, and J. He, "An improved grid current and DC capacitor voltage balancing method for three-terminal hybrid AC/DC microgrid," *IEEE Trans. Smart Grid*, to be published, doi: 10.1109/TSG.2018.2834340.

[4] J. C. Vasquez, J. M. Guerrero, A. Luna, P. Rodriguez, and R. Teodorescu, "Adaptive droop control applied to voltage-source inverters operating in grid-connected and islanded modes," *IEEE Trans. Ind. Electron.*, vol. 56, no. 10, pp. 4088–4096, Oct. 2009.

[5] Q.-C. Zhong and Y. Zeng, "Universal droop control of inverters with different types of output impedance," *IEEE Access*, vol. 4, pp. 702–712, Feb. 2016.

[6] J. Rocabert, A. Luna, F. Blaabjerg, and P. Rodríguez, "Control of power converters in AC microgrids," *IEEE Trans. Power Electron.*, vol. 27, no. 11, pp. 4734–4739, Nov. 2012.

[7] K. De Brabandere, B. Bolsens, J. Van den Keybus, A. Woyte, J. Driesen, and R. Belmans, "A voltage and frequency droop control method for parallel inverters," *IEEE Trans. Power Electron.*, vol. 22, no. 4, pp. 1107–1115, Jul. 2007.

[8] J. Yang, W. Yuan, Y. Sun, H. Han, X. Hou, and J. M. Guerrero, "A novel quasi-master-slave control frame for PV-storage independent microgrid," *Int. J. Elect. Power Energy Syst.*, vol. 97, no. 99, pp. 262–274, Apr. 2018.

[9] L. Fan and Z. Miao, "An explanation of oscillations due to wind power plants weak grid interconnection," *IEEE Trans. Sustain. Energy*, vol. 9, no. 1, pp. 488–490, Jan. 2018.

[10] F. Blaabjerg, R. Teodorescu, M. Liserre, and A. V. Timbus, "Overview of control and grid synchronization for distributed power generation systems," *IEEE Trans. Ind. Electron.*, vol. 53, no. 5, pp. 1398–1409, Oct. 2006.
[11] J. J. Justo, F. Mwasilu, J. Lee, and J.-W. Jung, "AC-microgrids versus DC-microgrids with distributed energy resources: A review," *Renew. Sustain. Energy Rev.*, vol. 24, pp. 387–405, Aug. 2013.
[12] X. Zhang, Q.-C. Zhong, V. Kadirkamanathan, J. He, and J. Huang, "Source-side series-virtual-impedance control to improve the cascaded system stability and the dynamic performance of its source converter," *IEEE Trans. Power Electron.*, to be published, doi: 10.1109/TPEL.2018.2867272.
[13] Q.-C. Zhong, W.-L. Ming, and Y. Zeng, "Self-synchronized universal droop controller," *IEEE Access*, vol. 4, pp. 7145–7153, 2016.
[14] Y. Sun, X. Hou, J. Yang, H. Han, M. Su, and J. M. Guerrero, "New perspectives on droop control in AC microgrid," *IEEE Trans. Ind. Electron.*, vol. 64, no. 7, pp. 5741–5745, Jul. 2017.
[15] J. M. Guerrero, L. Garcia de Vicuna, J. Matas, M. Castilla, and J. Miret, "Output impedance design of parallel-connected UPS inverters with wireless load-sharing control," *IEEE Trans. Ind. Electron.*, vol. 52, no. 4, pp. 1126–1135, Aug. 2005.
[16] J. He and Y. W. Li, "Analysis, design, and implementation of virtual impedance for power electronics interfaced distributed generation," *IEEE Trans. Ind. Appl.*, vol. 47, no. 6, pp. 2525–2538, Nov. 2011.
[17] H. Han, X. Hou, J. Yang, J. Wu, M. Su, and J. M. Guerrero, "Review of power sharing control strategies for islanding operation of AC microgrids," *IEEE Trans. Smart Grid*, vol. 7, no. 1, pp. 200–215, Jan. 2016.
[18] Y. Deng, Y. Tao, G. Chen, G. Li, and X. He, "Enhanced power flow control for grid-connected droop-controlled inverters with improved stability," *IEEE Trans. Ind. Electron.*, vol. 64, no. 7, pp. 5919–5929, Jul. 2017.
[19] F. Tang, J. M. Guerrero, J. C. Vasquez, D. Wu, and L. Meng, "Distributed active synchronization strategy for microgrid seamless reconnection to the grid under unbalance and harmonic distortion," *IEEE Trans. Smart Grid*, vol. 6, no. 6, pp. 2757–2769, Nov. 2015.
[20] Z. Shuai, W. Huang, X. Shen, Y. Li, X. Zhang, and J. Shen, "A maximum power loading factor (MPLF) control strategy for distributed secondary frequency regulation of islanded microgrid," *IEEE Trans. Power Electron.*, to be published, doi: 10.1109/TPEL.2018.2837125.
[21] X. Dou *et al.*, "A distributed voltage control strategy for multi-microgrid active distribution networks considering economy and response speed," *IEEE Access*, vol. 6, pp. 31259–31268, 2018, doi: 10.1109/ACCESS.2018.2837082.
[22] Y. Han, K. Zhang, H. Li, E. A. A. Coelho, and J. M. Guerrero, "MAS-based distributed coordinated control and optimization in microgrid and microgrid clusters: A comprehensive overview," *IEEE Trans. Power Electron.*, vol. 33, no. 8, pp. 6488–6508, Aug. 2018.
[23] C. Cho, J.-H. Jeon, J.-Y. Kim, S. Kwon, K. Park, and S. Kim, "Active synchronizing control of a microgrid," *IEEE Trans. Power Electron.*, vol. 26, no. 12, pp. 3707–3719, Dec. 2011.
[24] T. M. L. Assis and G. N. Taranto, "Automatic reconnection from intentional islanding based on remote sensing of voltage and frequency signals," *IEEE Trans. Smart Grid*, vol. 3, no. 4, pp. 1877–1884, Dec. 2012.
[25] A. Bellini, S. Bifaretti, and F. Giannini, "A robust synchronization method for centralized microgrids," *IEEE Trans. Ind. Appl.*, vol. 51, no. 2, pp. 1602–1609, Mar./Apr. 2015.
[26] A. Bidram and A. Davoudi, "Hierarchical structure of microgrids control system," *IEEE Trans. Smart Grid*, vol. 3, no. 4, pp. 1963–1976, Dec. 2012.
[27] J. M. Guerrero, J. C. Vasquez, J. Matas, L. G. de Vicuna, and M. Castilla, "Hierarchical control of droop-controlled AC and DC microgrids—A general approach toward standardization," *IEEE Trans. Ind. Electron.*, vol. 58, no. 1, pp. 158–172, Jan. 2011.
[28] D. E. Olivares *et al.*, "Trends in microgrid control," *IEEE Trans. Smart Grid*, vol. 5, no. 4, pp. 1905–1919, Jul. 2014.
[29] P. Wang, J. Xiao, and L. Setyawan, "Hierarchical control of hybrid energy storage system in DC microgrids," *IEEE Trans. Ind. Electron.*, vol. 62, no. 8, pp. 4915–4924, Aug. 2015.
[30] J. Wang, C. Jin, and P. Wang, "A uniform control strategy for the interlinking converter in hierarchical controlled hybrid AC/DC microgrids," *IEEE Trans. Ind. Electron.*, vol. 65, no. 8, pp. 6188–6197, Aug. 2018.
[31] L. Che, M. Shahidehpour, A. Alabdulwahab, and Y. Al-Turki, "Hierarchical coordination of a community microgrid with AC and DC microgrids," *IEEE Trans. Smart Grid*, vol. 6, no. 6, pp. 3042–3051, Nov. 2015.
[32] M. H. Cintuglu, T. Youssef, and O. A. Mohammed, "Development and application of a real-time testbed for multiagent system interoperability: A case study on hierarchical microgrid control," *IEEE Trans. Smart Grid*, vol. 9, no. 3, pp. 1759–1768, May 2018.
[33] Y. Han, H. Li, P. Shen, E. A. A. Coelho, and J. M. Guerrero, "Review of active and reactive power sharing strategies in hierarchical controlled microgrids," *IEEE Trans. Power Electron.*, vol. 32, no. 3, pp. 2427–2451, Mar. 2017.
[34] X. Hou, H. Han, C. Zhong, W. Yuan, Y. Sun, and M. Su, "A unified distributed control for grid-connected and islanded modes in multi-bus AC microgrid," in *Proc. Annu. Conf. IEEE Ind. Electron. Soc. (IECON)*, Beijing, China, 2017, pp. 2377–2382.
[35] H. Han, Y. Liu, Y. Sun, M. Su, and J. M. Guerrero, "An improved droop control strategy for reactive power sharing in islanded microgrid," *IEEE Trans. Power Electron.*, vol. 30, no. 6, pp. 3133–3141, Jun. 2015.
[36] X. Sun, Y. Tian, and Z. Chen, "Adaptive decoupled power control method for inverter connected DG," *IET Renew. Power Gener.*, vol. 8, no. 2, pp. 171–182, Mar. 2014.
[37] M. Debasish, A. Chakrabarti, and A. Sengupta, *Power System Small Signal Stability Analysis and Control*. New York, NY, USA: Academic, 2014, ch. 5, pp. 119–143.
[38] H. Geng, S. Li, C. Zhang, G. Yang, L. Dong, and B. Nahid-Mobarakeh, "Hybrid communication topology and protocol for distributed-controlled cascaded H-bridge multilevel STATCOM," *IEEE Trans. Ind. Appl.*, vol. 53, no. 1, pp. 576–584, Jan./Feb. 2017.

XIAOCHAO HOU received the B.S. and M.S. degrees from the School of Information Science and Engineering, Central South University, Changsha, China, in 2014 and 2017, respectively, where he is currently pursuing the Ph.D. degree in power electronics and power transmission.

He is a joint Ph.D. student supported by the China Scholarship Council with the School of Electrical and Electronic Engineering, Nanyang Technological University. His research interests include renewable energy systems, distributed microgrid, and power-electronic-enabled power network.

YAO SUN received the B.S., M.S., and Ph.D. degrees from the School of Information Science and Engineering, Central South University, Changsha, China, in 2004, 2007, and 2010, respectively. He is currently with the School of Information Science and Engineering, Central South University, as a Professor.

His research interests include matrix converter, microgrid, and wind energy conversion system.

JINGHANG LU (S'14–M'18) received the B.Sc. degree in electrical engineering from the Harbin Institute of Technology, China, in 2009, the two M.Sc. degrees in electrical engineering from the Harbin Institute of Technology in 2011 and the University of Alberta, Canada, in 2014, and the Ph.D. degree in power electronics from Aalborg University, Aalborg, Denmark, in 2018.

He is currently a Research Fellow with Nanyang Technological University, Singapore. His research interests include uninterruptible power supply and microgrid.

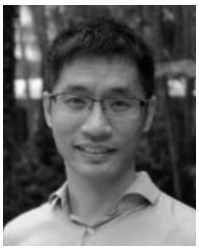

XIN ZHANG (M'15) received the Ph.D. degree in automatic control and systems engineering from The University of Sheffield, U.K., in 2016, and the Ph.D. degree in electronic and electrical engineering from the Nanjing University of Aeronautics and Astronautics, China, in 2014. He is currently an Assistant Professor of power engineering with the School of Electrical and Electronic Engineering, Nanyang Technological University. He was a Post-Doctoral Research Fellow with the City University of Hong Kong in 2017 and the Research Associate with The University of Sheffield from 2014 to 2016. He has received the highly prestigious Chinese National Award for Outstanding Students Abroad in 2016.

He is generally interested in power electronics, power system, and advanced control theory, together with their applications in various sectors.

LEONG HAI KOH received the B.Eng. degree (Hons.) and the Ph.D. degree in electrical engineering from Nanyang Technological University (NTU), Singapore, in 1994 and 2015, respectively. He is currently a Senior Scientist at the Energy Research Institute@NTU, Nanyang Technological University. His current research interests include smart grid, energy information and management system, hybrid ac/dc microgrid, renewable energy and integration, and power system modeling and simulation.

MEI SU received the B.S., M.S., and Ph.D. degrees from the School of Information Science and Engineering, Central South University, Changsha, China, in 1989, 1992, and 2005, respectively. Since 2006, she has been a Professor with the School of Information Science and Engineering, Central South University.

Her research interests include matrix converter, adjustable speed drives, and wind energy conversion system.

JOSEP M. GUERRERO (M'04–SM'08–F'15) received the B.S. degree in telecommunications engineering, the M.S. degree in electronics engineering, and the Ph.D. degree in power electronics from the Technical University of Catalonia, Barcelona, in 1997, 2000, and 2003, respectively.

Since 2011, he has been a Full Professor with the Department of Energy Technology, Aalborg University, Denmark, where he is responsible for the Microgrid Research Program. His research interests include different microgrid aspects, including power electronics, distributed energy-storage systems, hierarchical and cooperative control, and energy management systems.